Millimeter-wave MIMO: Wireless Links at Optical Speeds

Eric Torkildson, Bharath Ananthasubramaniam, Upamanyu Madhow, and Mark Rodwell

***Abstract*— We propose a new architecture for bridging the existing gap in speeds between wireless and optical links. The *Millimeter Wave MIMO* system employs "millimeter (mm) wave" spectrum in the E-band (70-95 GHz), which has been made available by the Federal Communications Commission on a semi-unlicensed basis for outdoor point-to-point communication. The small wavelengths enable highly directive beams providing link budgets sufficient to communicate even in poor weather conditions over ranges of the order of kilometers, while requiring radio frequency (RF) front-ends that can be realized in low-cost silicon processes. Furthermore, because of the small wavelengths, spatial multiplexing gains can be obtained even in Line of Sight (LOS) environments with only a moderate separation of transmitters. The proposed mm-wave Multiple-Input Multiple-Output system exploits these characteristics to provide LOS links of speeds of up to 40 Gbps (e.g., by supporting eight 5 Gbps links in parallel between two nodes). This paper provides an initial exposition of the key concepts, provides some rough calculations of attainable performance, and hints at the issues that must be addressed before this concept can become a reality.**

I. Introduction

The rapid strides in wireless communication in recent years has lead to inexpensive links with capacities in the 10s of Mbps, possibly approaching 100s of Mbps with the impending IEEE 802.11n Wireless Local Area Network standard. However, these speeds remain orders of magnitude smaller than the 10-160 Gbps speeds provided by optical links. In this paper, we propose an architecture for bridging this gap between wireless and optical link capacities in a cost-effective fashion. There are existing point-to-point wireless links that reach speeds of the order of Gbps. For example, a 1.25 Gbps point-to-point link using the 60 GHz band is reported in [6], and similar products are available in the marketplace [8], [1]. Our goal is to increase such data rates by more than an order of magnitude, to 10-40 Gbps. while at the same time simplifying installation. In addition to the natural application for communication infrastructure recovery after disasters, such wireless links offer tremendous commercial potential, as they can be used interchangeably with optical transmission equipment. For commercial applications, perhaps the greatest advantage of 10-40 Gbps wireless links is their lower cost, as they provide the bridge connections between optical links, where difficult terrains such as mountains and rivers are to be crossed, or where installation costs are prohibitive, as in city centers.

This research is supported by the National Science Foundation NSF under grants ECS-0636621, CNS-0520335 and CCF-0431205, and the DARPA SMART program.

The authors are with the Department of Electrical and Computer Engineering, University of California, Santa Barbara, CA 93106, USA.

We term our approach, depicted in Figure 1, Millimeter Wave MIMO. We propose to utilize millimeter (mm) wave frequencies in the E-band (71-95 GHz), where several large spectrum segments have been made available in a semi-unlicensed fashion by the FCC for point-to-point wireless communications. Use of the E-band avoids the high oxygen absorption characteristic of the 60 GHz unlicensed band, and enables ranges of the order of kilometers with reasonable transmit power. At these small wavelengths, it is possible to synthesize highly directive beams (which is an FCC requirement in the E-band) with moderately sized antennas, permitting significant spatial reuse and drastically limiting multipath. The key concepts behind the proposed system are as follows:

Adaptive beamforming: By making a highly directive beam (e.g. with a 1 degree beamwidth) steerable over a larger angle (say 10 degrees), we drastically simplify the task of installation. The directivity gains are obtained at both the transmitter and receiver by the use of adaptive antenna arrays, which we term *subarrays*.

Spatial multiplexing: The transmit and receive nodes each consist of an array of subarrays, as shown in Figure 1. After transmit and receive beamforming using the subarrays, each subarray can be interpreted as a single *virtual element* in a Multiple-Input Multiple-Output (MIMO) system. As a consequence of the small wavelength, moderate separation between the subarrays ensures that each virtual transmit element sees a different enough response at the virtual receive array. This enables spatial multiplexing: different virtual transmit elements can send different data streams, with a spatial equalizer at the virtual receive array used to separate the streams.

Example system: A speed of 40 Gbps over 1 km using 5 GHz of E-band spectrum can be achieved by using a 4×4 array of subarrays at each end, with the following parameters:

- Each parallel spatial link employs QPSK with 100% excess bandwidth, transmitting at 5 Gbps.
- An appropriately selected subset of 8 out of the 16 subarrays transmit parallel streams at 5 Gbps, resulting in an aggregate link speed of 40 Gbps.
- All 16 subarrays at the receiver are used in the spatial equalizer in order to separate out the 8 parallel data streams. Adequate spatial separation is achieved by spacing adjacent subarrays by about 0.7 meters, so that the transmit and receive nodes are each approximately of size 2 meters by 2 meters.

The signal processing underlying a mm-wave MIMO system, as in the preceding example, follows a natural two-level hierarchy. At Level 1, each subarray at the transmitter

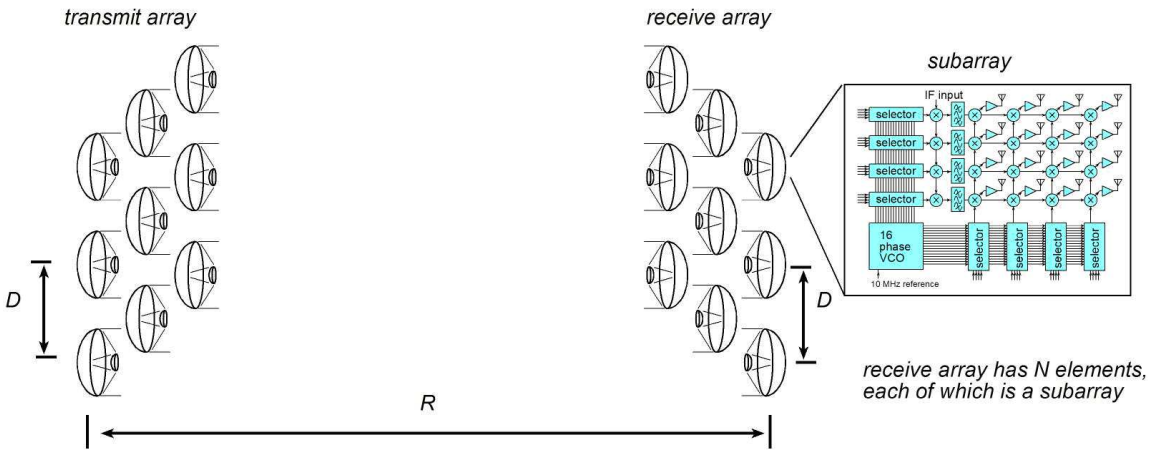

Fig. 1. Overview of the proposed 10-40 Gbps mm-wave MIMO system for integrating wireless and optics infrastructures. Each node consists of an array of subarrays. Each subarray in a node steers a beam towards the node it is communicating with, providing beamforming gain and ISI reduction.

synthesizes a beam to point towards the receiver, and each subarray at the receiver synthesizes a beam to point towards the transmitter. Once these beams have been formed, we must now perform Level 2 signal processing for the resulting virtual MIMO system. In the example above, this might correspond to a 16-tap zero-forcing spatial equalizer for each of the 8 transmitted data streams.

Our claim that cost-effective realizations of mm-wave MIMO systems are possible rests on ongoing advances in CMOS VLSI for implementing mm-wave radio frequency (RF) circuits, as well as low-cost packaging techniques. In addition, unlike lower-speed wireless systems in which Digital Signal Processing (DSP) takes over at a relatively early stage, the high speeds at which we operate demand the use of hybrid analog/digital signal processing algorithms which are co-designed with the hardware. In this paper, we aim to convey the following aspects of mm-wave MIMO systems: the architecture, some rough calculations on achievable performance, and an example of signal processing and hardware co-design for achieving electronic beamsteering.

It is worth putting our work in the context of the existing literature on MIMO, or space-time communication, which is a broad term encompassing different techniques for using multiple antennas at the transmitter and/or receiver. Beamforming and diversity using receive antenna arrays are a classical concept in communication theory, but the important role played by transmit antenna arrays, when used in conjunction with receive arrays, was pointed out by the pioneering work of Telatar[9] and Foschini[3]. Since then, three major concepts for utilizing transmit antenna arrays have emerged: Spatial Diversity, Spatial Multiplexing and Transmit Beamforming. Mm-wave MIMO differs fundamentally from MIMO systems at lower frequencies in several respects. First, the channels are LOS or near-LOS, hence *beamforming* rather than diversity is the appropriate strategy. Second, *spatial multiplexing* can no longer rely on rich scattering. Instead, it is obtained by focusing the receive antenna array on the different transmit antenna elements.

Level 1 signal processing for beamforming in discussed in Section II, where we provide an example of signal processing and hardware co-design. Beamforming can be performed on the complex envelope or on the passband signal, and at small operating bandwidths, baseband beamforming using DSP is often preferred. However, analog-to-digital conversion of a signal with 5 GHz bandwidth at sufficient precision for beamforming on the complex envelope is infeasible with current technology. We therefore consider an architecture for Level 1 beamforming which combines up/down conversion with antenna phase selection. We also provide an example link budget for the link obtained after level 1 beamforming. This provides the baseline for the performance estimates in Section III, where we describe the spatial multiplexing geometry at Level 2, which is the key to the increased data rates we promise. It is shown that a feasible link budget can be obtained despite suboptimal design choices, such as the use of uncoded QPSK and zero-forcing equalization. The penalties due to these choices relative to Shannon-theoretic limits are discussed. Finally, in Section IV, we discuss some of the many technical issues that must be addressed in order to realize the vision presented in this paper.

II. Beamforming for a single link

The basic building block of this MIMO system is a monolithic beamsteering IC (MBIC), which is the CMOS realization of a steerable subarray. Each MBIC electronically steers an $M \times M$ antenna array with element spacing d as shown in Figure 1, where the required M is estimated to be 4–10. This subarray is capable of achieving a directivity accuracy of less than 1 degree after initial manual positioning to within 10 degrees of the desired direction. This directivity cannot be obtained from a $M \times M$ half-wavelength spaced array at mm-wave. The antenna directivity is proportional to its effective aperture (see Section II-C). The effective aperture of the subarray can be increased using a telescopic dish configuration or a planar printed circuit board implementation (see Figure 2), while maintaining the steerability of the antenna. This provides the necessary beamforming gains to offset the higher attenuation in mm-waves and can be

used to suppress multipath to the extent possible. In addition, this directivity enables operation under the FCC mandate for E-band point-to-point links.

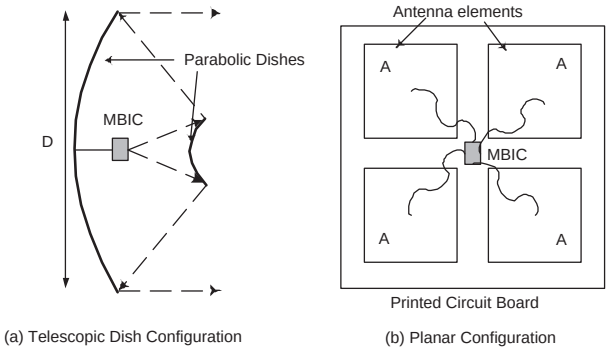

(a) Telescopic Dish Configuration (b) Planar Configuration

Fig. 2. Steerable Subarray Configurations

A. Row-Column Beamsteerer

While phased arrays at lower speeds can employ complex-valued beamforming weights at baseband, such approaches do not scale to the symbol rates and carrier frequencies of interest in this paper. We therefore present a row-column beamsteering IC, as depicted in Figure 5, in which two multi-phase local oscillators are mixed to synthesize the mm-wave carrier for each antenna element. Thus, the phase of the (i,j)th element of the array is given by

$$\phi(i,j) = \phi_h(i) + \phi_v(j), \quad 1 \le i,j \le M, \tag{1}$$

where $\phi_h(i)$ is the phase for the ith row, and $\phi_v(j)$ is the phase for the jth column, both chosen from a discrete set of values distributed uniformly around the unit circle. This then forms a hardware constraint for the signal processing algorithms discussed in Section IV. For the far-field regime we work in, the transmit subarrays beamform towards the receiver subarrays and vice-versa at the receiver, which can be accomplished efficiently using a two parameter search over the discrete set.

A special case of the row-column beamsteerer occurs when both the horizontal and vertical phases obey a linear profile, corresponding to steering a linear array in a specific direction. That is, $\phi_h(i) = i\delta_h$, and $\phi_v(j) = j\delta_v$, where $\delta_h = \frac{2\pi \sin\theta_h}{\lambda}$ and $\delta_v = \frac{2\pi \sin\theta_v}{\lambda}$ are the phase shifts for adjacent horizontal and vertical elements, respectively, corresponding to a horizontal steering angle of θ_h and a vertical steering angle of θ_v. Here the phase increments δ_h and δ_v must also be chosen from the discrete set allowed by our hardware constraints (i.e. phase increments of $\pi/4$ or $\pi/8$, corresponding to the use of 8- and 16-phase oscillators, respectively). The minimum phase increment corresponds to the desired resolution in steering angle. In Figures 3 and 4, the beamforming performance of a 4×4 $\lambda/2$-spaced array with 4-ary and 8-ary phase quantization for horizontal and vertical steering are shown. The plot represents the actual beamforming gain in dB along every direction in one quadrant seen as a projection on a unit sphere. The maximum

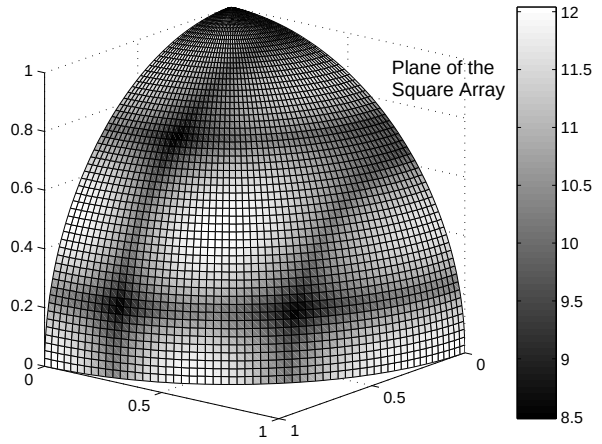

Fig. 3. Beamforming gains (in dB) from a 4×4 Row-Column Beamsteerer with linear profile and 4-ary phase quantization. One quadrant of the beampattern is shown on a unit sphere with actual gains (in dB) mapped using gray-scale.

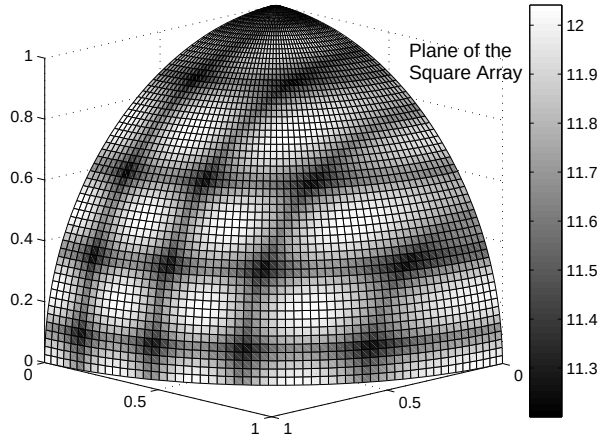

Fig. 4. Beamforming gains (in dB) from a 4×4 Row-Column Beamsteerer with linear profile and 8-ary phase quantization. One quadrant of the beampattern is shown on a unit sphere with actual gains (in dB) mapped using gray-scale.

achievable gain using a 4×4 square array is 12 dB and the worst case loss due to discretization is only about 4 dB even with 4-level discretization, which reduces to less than 1 dB for 8-level discretization. Since we are forming a single beam rather than trying to collect energy from several paths coming from different directions, a linear phase profile is adequate for our purpose.

B. CMOS IC Design

The MBIC subarrays process signals at both the RF ($\sim$71-95 GHz) and at the IF (5-10 GHz). Although our array configuration provides substantial multipath suppression when operating with highly directional beams, residual cross-channel ISI is still present. This can be corrected at the RF front-end by utilizing time- or frequency-domain

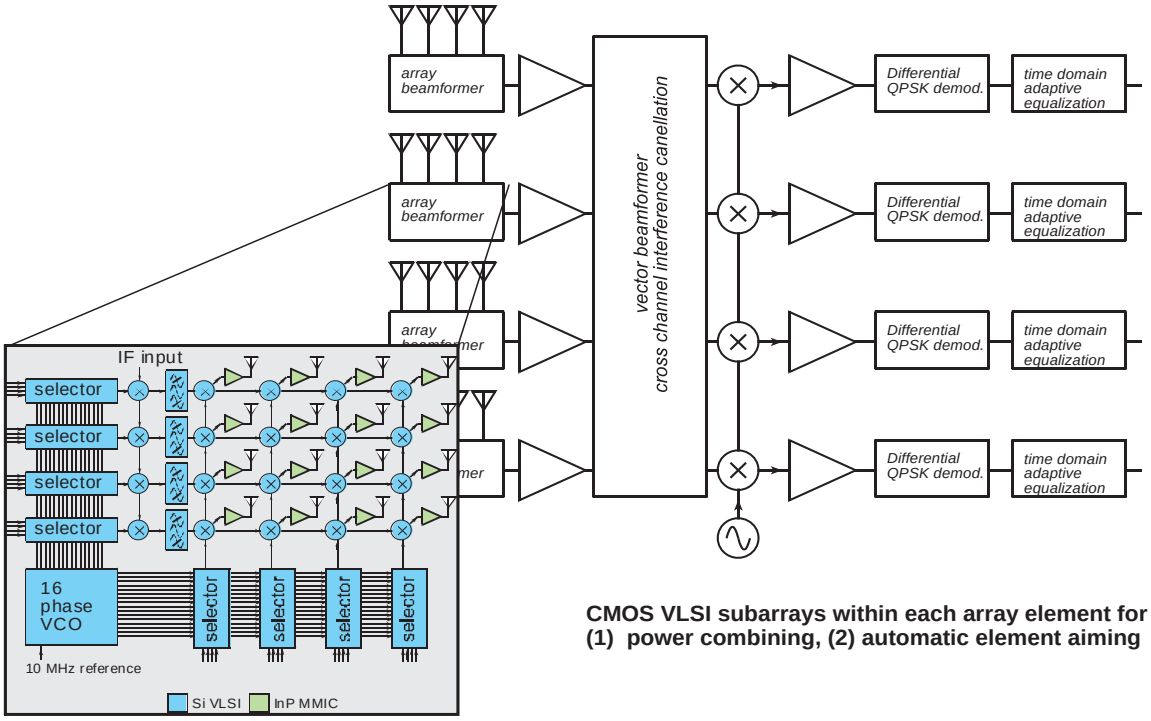

Fig. 5. Detailed description of the row-column beamsteering array VLSI.

adaptive equalization in either decision feedback or feed-forward format. Circuits to perform beamforming and sub-Rayleigh spatial equalization are designed to operate at the IF to reduce design complexity and power dissipation. The adaptive beamformer and equalizer can be realized as an adjustable vector summation network, which is implemented as DAC-controlled modulators with input control signals supplied by the baseband digital signal processor.

The above circuit functions are replicated in an array format (see block diagram in Figure 5) to support a $M \times M$ antenna matrix. Consequently, the highly regular floor plan of the the top-level layout of the MBIC eases the chip-to-board interface design and thus accommodate the matching networks for the antenna matrix. This high level of parallelism and complexity makes CMOS technology the only viable implementation choice. The key advantage of using CMOS for mm-wave systems up to 100 GHz is in fact its capability to integrate massively parallel transceiver arrays for directivity gain and adaptive beamforming. The MBICs are already in early development at UCSB using a 90-nm CMOS technology[2]. Preliminary system level simulation shows a 90-dB gain with a 32x32 overall array - 4x4 MBICs with each one supporting an 8x8 antenna matrix.

C. Baseline Link Budget

The MBIC enables us to adaptively synthesize a highly directive beam at both a transmit and receive subarray, without the requirement for accurate manual pointing. The resulting link is equivalent to an LOS fix-aimed link with small angular beamwidth. We now describe the link budget for such a link, e.g., between two buildings separated by a distance R with one subarray on each building. The transmitting and receiving antennas have effective apertures, A_t and A_r respectively. The antenna gains (directivities) are $G_t = 4\pi A_t/\lambda^2$ and $G_r = 4\pi A_r/\lambda^2$, where λ is the carrier wavelength. The received power according to the Friis' transmission equation is

$$\frac{P_{rec}}{P_{trans}} = \frac{G_t G_r \lambda^2}{16\pi^2 R^2} e^{-\alpha R}.$$

Under foul weather conditions, the atmospheric attenuation $\exp(-\alpha R)$ dominates over $(\lambda/R)^2$ in transmission losses; α is given for fair-weather conditions by Wiltse [10], rain attenuation is given in Olsen[7], and rain rate statistics by Karasawa[4]. Assuming quadrature-phase-shift-keying (QPSK) modulation, the minimum received power to support a B bit-rate link is $P_{rec} = Q^2 k_B T F B$, where $Q = 6$ for 10^{-9} uncoded bit error rate, k_B is the Boltzmann constant, T is the temperature and F is the received noise figure.

Consider a single subarray to subarray link operating at 75 GHz using a signal bandwidth of 5 GHz. Each 4×4 subarray is mounted on 30 cm diameter dish antennas (with a beamwidth of 2°) to boost its effective apertures to obtain a directivity of 45 dB while still maintaining the electronic steerability over 10°. Using the above relationships, for QPSK modulation (with 100% excess bandwidth) and a 6.5 dB receiver noise figure, a 5 Gbps link over a 1 km range, even in heavy 25 mm/hr rain, can be maintained with only

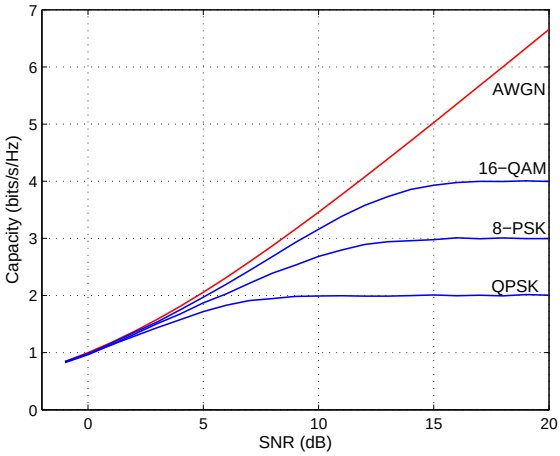

Fig. 6. Capacity of the single point-point link for different modulation schemes

160 mW transmit power at each subarray. This translates to 10 mW per element of the 4×4 subarray and also affords a link margin of 25 dB. The link margin can be used to operate such links even in the presence of significant spatial interference.

Once we layer spatial multiplexing on top of this at Level 2, one suboptimal approach is to use zero forcing spatial equalization to null out interference between different transmitting subarrays. In this case, the resulting noise enhancement would be subtracted from the link budget. For example, according to the preceding calculations, we can afford 15 dB of noise enhancement while still maintaining a link margin of 10 dB. On the other hand, additional gain due to receive spatial processing at Level 2 must be added to the link budget. The next section contains an example of such adjustments to the baseline link budget (see Section III-C).

III. Spatial Multiplexing at Level 2

The MIMO antenna is an array of monolithic subarrays (see Figure 1). Spatial multiplexing is obtained by focusing the receive subarrays on the different transmit subarrays. Once the subarrays beamsteer along the desired direction, they can be considered antenna elements of a virtual MIMO system. An $N \times N$ array of subarrays with lateral spacing D has dimensions $(N-1)D \times (N-1)D$. To realize the desired spatial multiplexing, each of the N^2 virtual transmit elements must see a sufficiently different N^2-ary (virtual) receive array response, in order to be able to separate out the different transmitted streams. The Rayleigh criterion in imaging [5] determines the minimum spacing between transmit elements so that they can be resolved by the receive array without any cross-talk. We are interested, however, in allowing for sub-Rayleigh spacing, hence we now derive the correlation between the responses at the receiver to two different (virtual) transmit elements. We illustrate the computations involved for uniform linear arrays (ULA) aligned to the broadside of each other, as displayed in Figure 7.

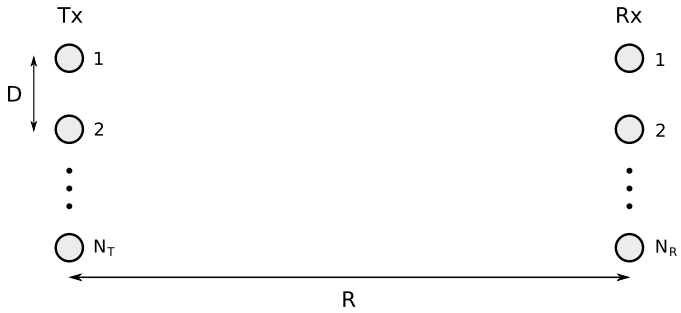

Fig. 7. Geometry of the linear array MIMO system at Level 2.

A. Rayleigh Spacing

The distance between the transmitter and receiver is R. The transmitter has N_T elements, and the receiver has N_R elements, where these (virtual) elements are actually subarrays. The path difference between adjacent receive elements is given by $\Delta L = \sqrt{D^2 + R^2} - R \approx \frac{D^2}{2R}$, with a corresponding phase difference of

$$\phi = \frac{2\pi}{\lambda} \Delta L \approx \frac{\pi}{\lambda} \frac{D^2}{R}, \tag{2}$$

where λ is the wavelength of the carrier wave. The receiver array response to transmit (Tx) element 1 is given by $\mathbf{a_1} = [1 \; e^{j\phi} \; e^{j2^2\phi} \; \ldots \; e^{j(N_R-1)^2\phi}]$ and the response to Tx element 2 is given by $\mathbf{a_2} = [e^{j\phi} \; 1 \; e^{j\phi} \; e^{j2^2\phi} \; \ldots \; e^{j(N_R-2)^2\phi}]$. After applying some algebraic manipulation and Euler's formula, the correlation between these two array responses is found to be:

$$\rho = \frac{|\mathbf{a_1}^{\mathrm{H}} \mathbf{a_2}|}{\|\mathbf{a_1}\| \, \|\mathbf{a_2}\|} = \frac{\sin(N_R \phi)}{N_R \sin(\phi)},$$

where $\mathbf{a_1}^{\mathrm{H}}$ denotes the conjugate transpose of $\mathbf{a_1}$. The correlation is driven to zero (and different elements at the transmitter can be resolved at the receiver), when $N_R \phi = \pi$. Applying (2), we obtain the same condition as the Rayleigh criterion:

$$D = \sqrt{\frac{R\lambda}{N_R}}, \tag{3}$$

which is the diffraction-limited resolution of an optical system. Any integer multiple of this spacing is also adequate to null the cross-talk. Thus the Rayleigh criterion spacing suppresses the spatial interference from the transmitter completely and eliminates the need for spatial equalization when $N_T \leq N_R$. In fact, careful analysis using Gaussian beams [11] shows that the Rayleigh criterion $D = \sqrt{R\lambda/N}$ holds when applied to $N \times N$ square transmit and receive arrays as well.

For a uniform linear receive array with $N_R = 16$, carrier frequency $f_c = 75$ GHz, and range $R = 1$ km, the Rayleigh criterion is satisfied at $D = 0.5$ m, leading to an overall array length of 7.5 m. Alternatively, the 16 elements can be arranged in a 4 $\times$ 4 square array, resulting in $D = 1$ m, a side length of $(N-1)D = 3$ m and a total area of $9\mathrm{m}^2$. These dimensions can be reduced further in order to obtain more compact nodes by using a sub-Rayleigh spacing

between adjacent elements. The resulting cross-talk can be addressed, for example, by the use of a spatial equalizer at the receiver. The effects of sub-Rayleigh spacing on system performance are examined in detail in Section III-C.

B. MIMO Capacity and Noise Enhancement

Consider a mm-wave MIMO system with N_T transmit elements and N_R receive elements (at Level 2). Assuming no temporal inter-symbol interference (which is a good approximation, given the narrow beams synthesized at Level 1), the $N_R \times 1$ received signal vector $\mathbf{y}$ is given by:

$$\mathbf{y} = \mathbf{H}\mathbf{x} + \mathbf{n}, \tag{4}$$

where $\mathbf{x}$ is the $N_T \times 1$ transmitted vector and $\mathbf{n}$ is an $N_R \times 1$ vector of independent identically distributed zero-mean circularly symmetric complex white Gaussian noise. $\mathbf{H}$ is the $N_R \times N_T$ channel matrix with entries $h_{m,n}$ corresponding to the complex channel gain from the mth transmit element to the nth receive element. In this paper, we only consider configurations where the plane of the transmit and receive arrays are parallel to each other. Since, we assume a LOS channel with no signal path loss (the loss is accounted for in the link budget), it is sufficient to examine the normalized channel matrix for the capacity and noise enhancement calculations that follow. The elements of the (normalized) channel matrix are:

$$\tilde{h}_{m,n} = e^{-i\frac{2\pi}{\lambda}(d(m,n)-R)}, \tag{5}$$

where λ is the carrier wavelength, $d(m,n)$ is distance between the mth transmit and nth receive elements, and R is the distance between the transmit and receive arrays, as measured from their centers. Note that $\mathbf{H}$ is a deterministic function of the geometry of the MIMO system due to the LOS nature of the channel and depends only on the difference in propagation distance between elements.

The channel capacity corresponding to a MIMO channel matrix, derived by Telatar in [9], is

$$C = \sum_{i=1}^{n} \log\left(1 + \frac{P_i \lambda_i^2}{N_0}\right) \text{bits/s/Hz}, \tag{6}$$

where n is the number of singular values of channel matrix $\mathbf{H}$, λ_i is the ith singular value of $\mathbf{H}$ and P_i is the power allocation provided to the ith eigenchannel satisfying $\sum_i P_i \leq P$.

Two power allocation policies are considered in this paper: water-filling allocation and equal power allocation. The optimal strategy of water-filling power allocation is achieved when P_i is given by:

$$P_i = \left(\mu - \frac{N_0}{\lambda_i^2}\right)^+, \tag{7}$$

where a^+ indicates $\max\{0, a\}$. The value of μ is chosen such that $\sum_i P_i = P$, where P is the total transmit power. To achieve the water-filling capacity, knowledge of the channel matrix must be available to the transmitter. If this knowledge is unavailable, equal power allocation is used, where $P_i = P/n$.

In sub-Rayleigh spaced arrays, spatial interference between transmit elements necessitates the use of spatial equalization at the receiver. In this paper, we consider linear zero-forcing (ZF) equalization when independent streams are sent from each transmit element with equal power (not capacity achieving for sub-rayleigh spacing), and evaluate its performance using the noise enhancement as the measure. The ZF vector for the ith transmit element is given by:

$$\mathbf{c}_i = \mathbf{H}\left(\mathbf{H}^H\mathbf{H}\right)^{-1}\mathbf{e}_i, \tag{8}$$

where $\mathbf{e}_i^T = (0, 0, ..., 1, ..., 0)$ and $i = 1, ..., N_T$. The noise enhancement for the ith transmit element is given by:

$$\eta_i = 10\log_{10}(\|\mathbf{c}_i\|^2\|\mathbf{h}_i\|^2) \tag{9}$$

Noise enhancement tends to be higher for a given transmit element when the number of neighboring elements is high or their proximity is close. Thus, transmit elements at the center of a linear or square array incur higher noise enhancement.

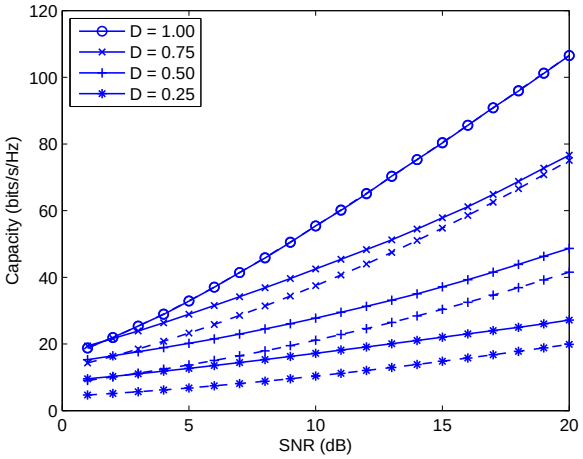

Fig. 8. 4 x 4 array Capacity versus SNR for different normalized Rayleigh spacings: Comparison of optimal water-filling capacity (solid lines) and ZF equalization (dashed lines) with independent streams on each transmit element.

The design choices we are currently considering are severely suboptimal, primarily because of implementation constraints. The first source of suboptimality is that we cannot support large constellations and channel coding at multiGigabit speeds (at least, we do not envision it for our first generation prototype). Thus, we consider uncoded QPSK in our baseline design. In this case, the spectral efficiency is 2 bps/Hz (not accounting for excess bandwidth), and the required SNR is 12.55 dB at BER of 10^{-9}. This is almost 11 dB away from AWGN capacity at 2 bps/Hz, while the AWGN capacity at 12.55 dB is 6 bps/Hz. We get optical link speeds despite this inefficiency by using large bandwidths (5 GHz) and spatial multiplexing (8-fold). The second source of suboptimality is the assumed use of zero-forcing equalization at the receiver: in Figure 8 the gap to capacity is due to this; the gap is much smaller than the one due to the use of small constellations without coding. Further,

this gap can be reduced by the use of more sophisticated MIMO techniques at Level 2 (e.g., linear transmit precoding along the channel eigenmodes, assuming channel feedback, or nonlinear cancellation techniques at the receiver), as we plan to explore in our future work.

C. Sample System Realizations

We now look 2 realizations of mm-wave MIMO: one with 16-element ULAs and the other 4×4 square arrays at the transmitter and receiver. The remaining system parameters are as described in Section II-C.

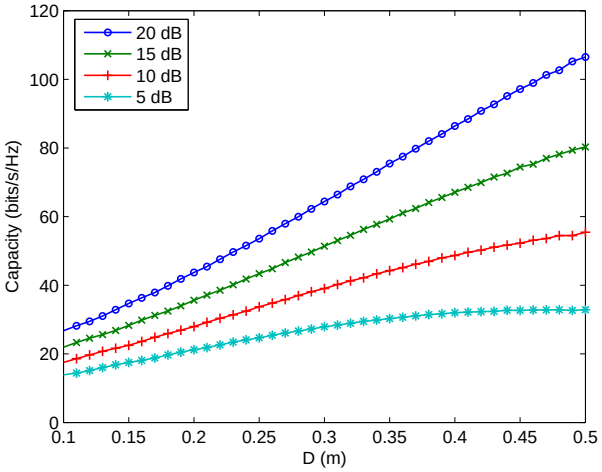

Fig. 9. 16-element ULA: Capacity vs. D under water-filling power allocation.

For the 16-element ULA, the Rayleigh spacing criterion is 0.5 m. We study first the effect of the inter-element spacing D and signal to noise ratio(SNR) on the Shannon capacity for the MIMO channel. The water-filling power allocation capacity as a function of the spacing, D, is shown in Figure 9 for several values of signal-to-noise ratio (SNR). At Rayleigh spacing, there is no spatial interference and capacity corresponding to a noise-limited system is obtained. But as D is decreased, the spatial interference increases (due to lack of separation between transmit elements seen from the receiver) and we reach an interference limited scenario with lower capacity. For the 4×4 square array, the Rayleigh spacing is 1 m – the Rayleigh criterion spacing of an $N \times N$ square array is larger than that of the N^2 element ULA by a factor $\sqrt{N}$. The capacity for the square array also behaves like the 16-element ULA and increases with spacing as seen in Figure 10. Although the capacity obtained using both array configurations are the same, the square array shows more variability with D as each element has a larger number of neighboring elements than the linear array. From Tables I and II, it is seen that square arrays provide the same capacity at roughly the same SNR while being more compact (side length) inspite of having a larger Rayleigh criterion spacing.

The performance of the ZF spatial equalizer can be measured using the noise enhancement (relative to the baseline

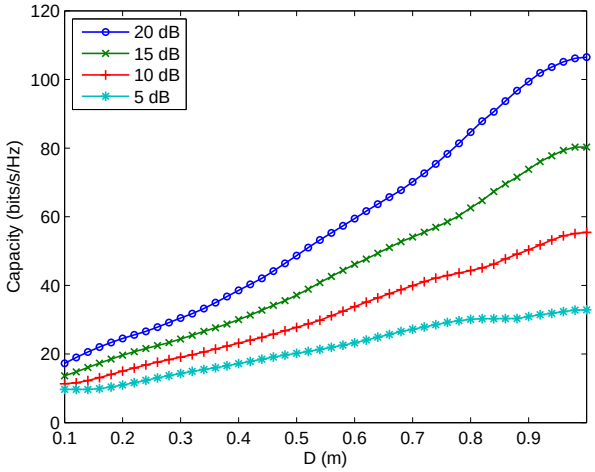

Fig. 10. 4x4 square array: Capacity vs. D under water-filling power allocation.

TABLE I

A SELECTION OF 16-ELEMENT ULA ARRAY CONFIGURATIONS

D (m)	Length (m)	Req. SNR (dB)	
		20 bps/Hz	30 bps/Hz
0.5	7.5	1.39	4.26
0.375	5.625	0.78	4.58
0.25	3.75	2.09	8.03
0.125	1.875	9.75	19.85

TABLE II

A SELECTION OF 4×4 ARRAY CONFIGURATIONS

D (m)	Side Length (m)	Req. SNR (dB)	
		20 bps/Hz	30 bps/Hz
1.00	3	1.39	4.26
0.75	2.25	1.25	5.43
0.50	1.5	4.86	11.27
0.25	0.75	12.92	22.43

of a single link). The noise enhancement quantifies loss in signal power due to perfect cancelation of the spatial interference vectors, which can be viewed as effective decrease in SNR. This noise enhancement is an upper bound on the gap to MIMO capacity (without knowledge of the channel at the transmitter). In Figures 11 and 12, the mean (averaged over the elements), maximum, and minimum noise enhancement is shown as a function of D for 16-element linear arrays and 4×4 square array.

A reduction in noise enhancement, at the cost of throughput, can be achieved by using a subset of the available transmit arrays. For example, Figure 14 shows the resulting noise enhancement when only a subset of the 4×4 array elements are transmitting. The two subsets are displayed in Figure 13. The ability to transmit over a subset of transmit elements provides added flexibility, allowing the mm-wave MIMO system to adapt to environmental conditions to remain operating within desired limits of data throughput or received signal strength. Further, the baseline system has a 25 dB margin and also gets a 16-fold (12 dB) gain from the use

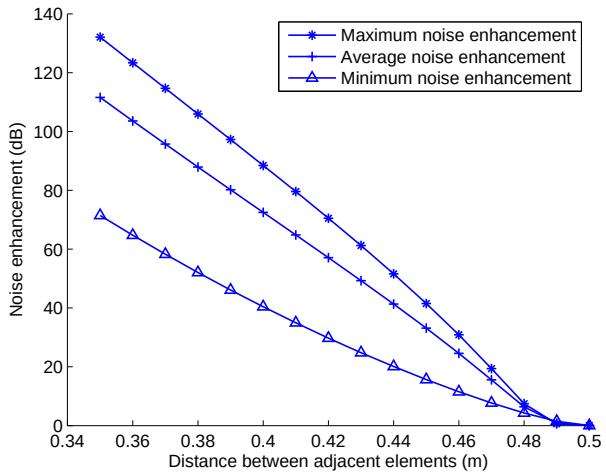

Fig. 11. Noise enhancement due to ZF equalization of 16-element linear array as a function of D.

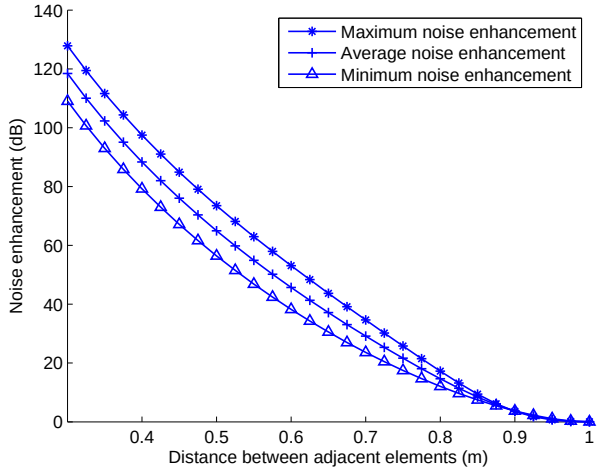

Fig. 12. Noise enhancement due to ZF equalization of 4x4 square array as a function of D.

of a 16 (4×4) receiver subarrays. From Figure 12, it is seen that a 30 dB (average) noise enhancement penalty is incurred when the inter-element spacing is about 0.65 m or 65% of the Rayleigh spacing. This effective decrease in received signal power (noise enhancement) due to the ZF equalization can be offset by increasing the transmit power, which is available to us in the form of the 37 dB link margin. Therefore, the system dimensions can be reduced by 35% while still achieving the maximum (Rayleigh spacing) capacity and leaving a 7 dB link margin. As mentioned earlier, this trade-off is very useful in keeping the array dimensions manageable. In this manner, we can trade-off power for greater operational range or smaller system dimensions.

We next look at the scaling of capacity with the number of MIMO antenna elements for the square array and ULA when the D is chosen to be half the Rayleigh criterion spacing. An equal increase in both N_T and N_R results in

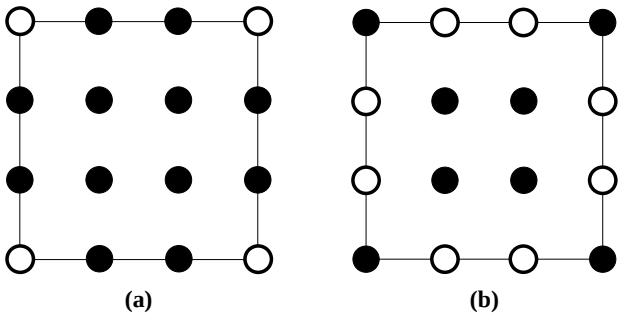

Fig. 13. (a) 4-element subset and (b) 8-element subset transmit array configurations. Black circles represent switched-off transmit elements.

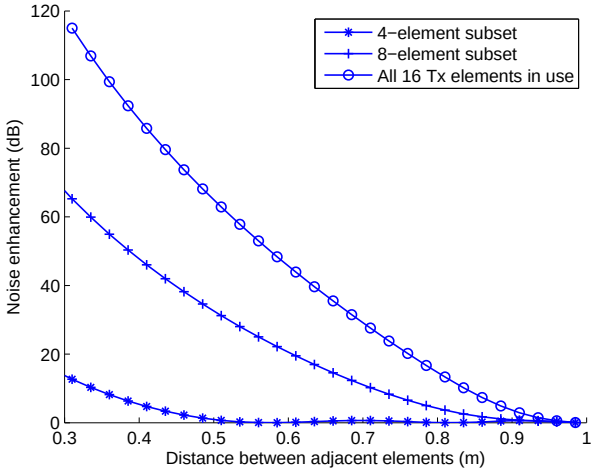

Fig. 14. Noise enhancement resulting when a subset of elements of the 4×4 array are in use. Subset configurations shown in Figure 13.

a linear increase in channel capacity, as illustrated in Figure 15. However, this increase in capacity is accompanied by the costs of larger physical dimensions, added spatial equalizer complexity, and greater noise enhancement resulting from linear spatial equalization.

IV. Future Work and Conclusions

The proposed mm-wave MIMO system leverages small wavelengths in two ways, high directivities can be obtained by moderate sized subarrays, and multiple spatial eigenmodes can be created in a LOS environment with relatively small separation between subarrays. The theoretical computations in this paper indicate the feasibility of low-cost realizations of this concept using emerging CMOS VLSI, since the transmit power requirements are moderate (less than 10 mW per subarray) for attaining 40 Gbps link speeds over a range of kilometers, with a link margin sufficient to overcome poor weather conditions. Our computations for various array geometries show that the nodes are of manageable size, of the order of a few meters in dimension. Comparison with Shannon-theoretic limits show that there is a substantial performance loss due to our suboptimal design choices. However, the attainable link budget, and the gains in spectral efficiency from spatial multiplexing, are such that

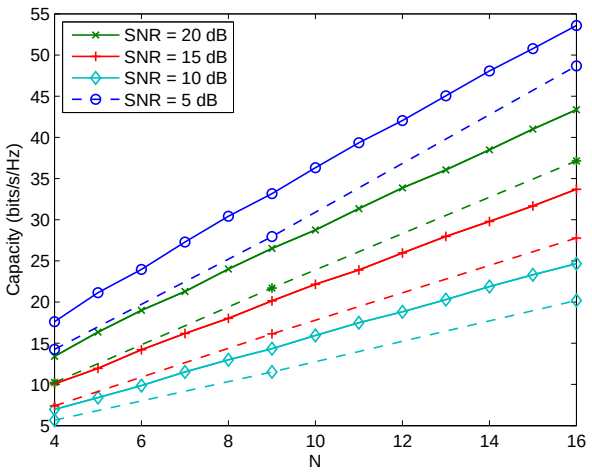

Fig. 15. Channel capacity vs. N for $D = 0.5D_R$ ($D_{square} = 0.5$ m, $D_{linear} = 0.25$ m). Dashed line represents square array results, defined only at N = {4, 9, 16}

there is sufficient margin that we can live with these choices.

We have now established the potential of the proposed architecture for realizing wireless links at optical speeds. The work of realizing this potential requires sustained effort in a number of areas, including CMOS VLSI design and packaging for mm-wave RF circuitry, hybrid digital/analog baseband algorithms and their CMOS realization, and protocols for automated link establishment, as well as integration of all of these technologies into a single system. Further work is also needed on characterizing multipath due to obstacles and ground reflections, and low-complexity techniques for handling it that can be realized at multiGigabit speeds.

REFERENCES

[1] Bridgewave-Communications, "60 Ghz Wireless Links for High-Bandwidth Data Application," http://www.winncom.com/pdf/AR60_Specs.pdf, 2005.

[2] C. Carta, M. Seo, and M. Rodwell, "A mixed-signal row/column architecture for very large monolithic mm-wave phased arrays," in *2006 IEEE Lester Eastman Conference On High Performance Devices.*, August 2006.

[3] G. Foschini, "Layered space-time architecture for wireless communications in a fading environment," *Bell Labs Technical Journal*, vol. 1, no. 2, pp. 41–59, Autumn 1996.

[4] Y. Karasawa and Y. Maekawa, "Ka-band Earth-space propagation research in Japan," in *Proc. IEEE*, vol. 85, no. 6, June 1997, pp. 821–842.

[5] J. D. Kraus, *Radio Astronomy*, 2nd ed. Cygnus-Quasar, 1986, pp. 6–19.

[6] K. Ohata, K. Maruhashi, M. Ito, S. Kishimoto, K. Ikuina, T. Hashiguchi, K. Ikeda, and N. Takahashi, "1.25 gbps wireless gigabit ethernet link at 60ghz-band," in *2003 IEEE MTT-S International Microwave Symposium Digest*, vol. 1, June 2003, pp. 373–376.

[7] R. Olsen, D. Rogers, and D. Hodge, "The aR^b relation in the calculation of rain attenuation," *IEEE Trans. Antennas Propagat.*, vol. 26, no. 2, 1978.

[8] Proxim-Wireless, "Gigalink Series – Alternative To Fiber Up To Gigabit Speeds," http://www.proxim.com/downloads/products/gigalink/DS_0806_GIGALINK_USHR.pdf, 2006.

[9] E. Telatar, "Capacity of multi-antenna Gaussian channels," *Tech. Report, AT&T Bell Labs*, 1995.

[10] J. C. Wiltse, "Corrections to published curves for atmospheric attenuation in the 10 to 1000 GHz region," in *IEEE Antennas and Propagation Society International Symposium Digest*, vol. 4, 1997, pp. 2580–2583.

[11] A. Yariv and P. Yeh, *Optical Waves in Crystals; Propagation and Control of Laser Radiation*. John Wiley & Sons, Inc., 2002.